

High-temperature argon broadening of CO₂ near 2190 cm⁻¹ in a shock tube

C. R. Mulvihill¹  · E. L. Petersen¹

Received: 21 July 2017 / Accepted: 12 September 2017 / Published online: 22 September 2017
© Springer-Verlag GmbH Germany 2017

Abstract Scanned-wavelength laser absorption measurements of CO₂ diluted in Ar were performed behind reflected shock waves at high temperatures (1158–2017 K) and low pressures (5.1–108.4 kPa). High-resolution (0.001 cm⁻¹) scans were conducted in 0.4-cm⁻¹ increments from about 2188.8 to 2191.8 cm⁻¹ at a scan rate of 2 kHz. The HITRAN 2004, HITRAN 2012, and CDSD-296 databases were all found to underestimate the absorption, typically by an order of magnitude or more. The HITEMP database, however, closely predicted the measured data. For the assumed form $\gamma_{\text{CO}_2\text{-Ar}}(T) = \gamma_{\text{CO}_2\text{-Ar}}(T_0)(T_0/T)^n$ with $T_0 = 296$ K, an optimization routine was implemented to determine the values of $\gamma_{\text{CO}_2\text{-Ar}}(T_0)$ and n . From the optimization, values of 0.033 ± 0.004 cm⁻¹ atm⁻¹ and 0.61 ± 0.04 were determined for $\gamma_{\text{CO}_2\text{-Ar}}(T_0)$ and n , respectively, which are in good agreement with historical values. These values describe an average CO₂-Ar broadening coefficient in the frequency range studied herein and are reliable within the experimental temperature range. In addition, a set of fixed-wavelength measurements at 2190.0175 cm⁻¹ were carried out at 122, 446, and 1115 kPa between 1100 and 2100 K, and the HITEMP predictions incorporating the proposed Ar-broadening parameters showed excellent agreement with these data.

1 Introduction

Carbon dioxide (CO₂) is a minor yet closely monitored atmospheric constituent as well as a primary byproduct of hydrocarbon combustion. Accurate spectroscopic information is often desirable for measuring CO₂ concentration in these applications, and thus, several spectroscopic databases on CO₂ have been compiled for ambient temperatures, including HITRAN 2004 [1], HITRAN 2012 [2], and CDSD-296 [3], among others. Databases have also been developed for high-temperature applications, including CDSD-1000 [4], CDSD-4000 [5], and HITEMP [6]. These databases contain line positions, linestrengths, and various broadening parameters pertaining to air- and self-broadening.

Laser absorption techniques play a large and growing role in gas-sensing measurements [7]. The high spatiotemporal coherence of lasers offers quantitative, spatially resolved measurements of species concentrations and temperatures. To attain reliable quantitative measurements for high-resolution spectroscopy, accurate parameters are needed to describe the broadening of the spectral lines of an absorbing species (an absorber) by a non-absorbing species (a perturber).

Argon (Ar) is often preferred as a shock-tube bath gas in chemical kinetics experiments, because it is chemically inert and because its high specific heat ratio mitigates reflected-shock bifurcation [8]. Since high dilution levels ($\geq 98\%$ by vol.) of Ar are typically used in shock-tube laser absorption experiments to limit the temperature rise due to exothermicity, Ar-broadening is often the dominant broadening mechanism. Therefore, obtaining accurate predictions of CO₂ absorption during shock-tube chemical kinetics experiments requires values of CO₂-Ar-broadening parameters that are valid at high temperatures (> 1000 K). None of

Electronic supplementary material The online version of this article (doi:10.1007/s00340-017-6830-8) contains supplementary material, which is available to authorized users.

✉ C. R. Mulvihill
cmulvihill@tamu.edu

¹ Department of Mechanical Engineering, Texas A&M University, 3123 TAMU, College Station, TX, USA

the previously mentioned spectral databases contains Ar-broadening data.

The ν_3 (asymmetric stretch) band of CO_2 manifests itself from about 2000 to 2500 cm^{-1} . Of interest to the authors is the overlap of the low-frequency wing of the ν_3 band of CO_2 with the fundamental band of CO. In a recent work from the authors' laboratory [9], interfering absorption from CO_2 had to be subtracted out from laser absorption measurements at the R(12), $\nu'' = 0$ line of CO at 2190.0175 cm^{-1} . This interference from CO_2 absorption was unexpected due to earlier calculations by Ren et al. [10] using HITRAN 2004 that suggested negligible absorption by CO_2 at this frequency (see Fig. 2 of [10]). Although HITEMP better predicts CO_2 absorption at high temperatures (see below), a need still exists for high-temperature CO_2 -Ar-broadening parameters near 2190 cm^{-1} . The subject of the present study, therefore, was to measure directly the CO_2 -Ar broadening at conditions of interest to shock-tube combustion studies. Provided in this paper, following a background section on relevant theory and literature, are details of the experimental setup. The results of the experiments and the suggested broadening parameters are covered in the last half of the paper.

2 Background

2.1 Theory

The absorption of monochromatic light is described by the Beer-Lambert relation:

$$I_t/I_0 = \exp[-S(T)\phi(\nu - \nu_0)PX_{\text{abs}}L], \quad (1)$$

which relates the incident and transmitted intensities I_0 and I_t to the linestrength $S(T)$ [$\text{cm}^{-2} \text{atm}^{-1}$], the lineshape function $\phi(\nu - \nu_0)$ [cm], the total pressure P [atm.], the mole fraction of the absorber X_{abs} , and the path length L [cm]. The linestrength S is a function of temperature T [K], while the lineshape ϕ is a function of T and P as well the distance $\nu - \nu_0$ from the line center ν_0 [cm^{-1}].

Various models can be used to describe ϕ ; combustion scientists often employ the Voigt profile. The Voigt profile is given as the convolution of the Doppler and Lorentzian profiles, which are themselves described by their full width at half maximum (FWHM) values $\Delta\nu_D$ and $\Delta\nu_L$ [cm^{-1}], given by

$$\Delta\nu_D = 7.162 \times 10^{-7} \nu_0 \sqrt{T/M} \quad (2)$$

and

$$\Delta\nu_L = \sum_j 2\gamma_{i-j}(T)PX_j. \quad (3)$$

Here, M is the molecular weight [g mol^{-1}], $\gamma_{i-j}(T)$ is the broadening coefficient of absorber i broadened by perturber

j [$\text{cm}^{-1} \text{atm}^{-1}$], and X_j is the mole fraction of perturber j . The summation in Eq. (3) extends over all perturbers, including the absorber itself (i.e., self-broadening). The temperature dependence of the broadening coefficient γ_{i-j} is assumed to follow the familiar power law:

$$\gamma_{i-j}(T) = \gamma_{i-j}(T_0)(T_0/T)^n \quad (4)$$

where $\gamma_{i-j}(T_0)$ is the broadening coefficient at reference temperature T_0 (herein, $T_0 = 296$ K), and n is the temperature exponent of the same $i-j$ system. Both $\gamma_{i-j}(T_0)$ and n are necessary to predict the broadening behavior of an absorber-perturber pair at high temperatures. The functional dependencies of $\gamma_{i-j}(T_0)$ and n are discussed more in the following sections.

2.1.1 Previous work concerning $\gamma_{\text{CO}_2\text{-Ar}}(T_0)$

At or near 296 K, CO_2 -Ar broadening has been investigated by a number of workers and in various vibrational bands. Boulet et al. [11] measured $\gamma_{\text{CO}_2\text{-Ar}}(T_0)$ at 296 K up to $J \approx 40$. Similar measurements were performed in the $3\nu_3$ band [12], the ν_3 band [13, 14], and the $3\nu_1 + \nu_3$ band [15]. A general consensus has been reached, based on theory and experiments, that there is no dependence of $\gamma_{\text{CO}_2\text{-j}}(T_0)$ on the vibrational band [16] as first suggested by Arié et al. [17]. As for rotational effects, the J'' -dependence of $\gamma_{\text{CO}_2\text{-Ar}}(T_0)$ has been well established [16, 18, 19].

Despite the considerable body of work on $\gamma_{\text{CO}_2\text{-Ar}}(T_0)$, no studies near 2190 cm^{-1} were found in the literature. The lack of activity at this frequency is likely due to the small linestrengths ($\sim 1 \times 10^{-5} \text{cm}^{-2} \text{atm}^{-1}$) at room temperature and the many overlapping hot bands at high temperatures (> 1000 K) that make measurements difficult to interpret. Furthermore, the prediction of broadening parameters using the known J'' -dependence of $\gamma_{\text{CO}_2\text{-Ar}}(T_0)$ is complicated by the many strong lines at high temperatures that muddle the definition of an effective J'' value. Thus, the present work aimed to measure $\gamma_{\text{CO}_2\text{-Ar}}(T_0)$ by making measurements at high temperatures near frequencies of 2190.0 cm^{-1} and extrapolating back to T_0 through use of the temperature exponent n .

2.2 Previous work concerning n

To obtain information on the temperature exponent n , Ar-broadening measurements and calculations have been performed at temperatures other than 296 K. This problem was first addressed by Pack [20], who assessed the temperature dependence of Ar- and He-broadened CO_2 lines via infinite-order sudden (IOS) calculations. Brownsword et al. [13] performed measurements at 160 and 300 K and reported $n = 0.88 \pm 0.18$. In an experimental and theoretical work between 77 and 765 K, Thibault et al. [18] reported a value

of $n = 0.70$ below 296 K and a value of 0.64 above 296 K. At higher temperatures, Wooldridge et al. [21] measured a value of $n = 0.61 \pm 0.01$ for the R(48), R(50), and R(52) lines of the ν_3 band from 296 to 2290 K, while Spearrin et al. [22] investigated several lines in the ν_3 and $\nu_1 + \nu_3$ bands from about 1000 to 2000 K. Farooq et al. [23] investigated two lines in the $\nu_1 + \nu_3$ band between 300 and 1200 K. The literature values of n are summarized in Table 1.

It is well known that n is itself a weak function of temperature [10, 18, 20] and that the power dependence given in Eq. (4) is typically only valid over a certain temperature range for a given value of n . The difference in the temperature ranges studied by Brownsword et al. [13] and Wooldridge et al. [21] is thus the likely explanation for the large discrepancy in their reported values of n . Similarly, Spearrin et al. [22] and Farooq et al. [23] both measured n for the R(28) line at 3633.08 cm⁻¹, but obtained noticeably different values, since their temperature ranges were different. Since both Spearrin et al. [22] and Wooldridge et al. [21] performed their measurements near the temperatures of the present study, it is expected that the value of n obtained herein should fall closer to their values.

3 Experimental setup

3.1 Shock tube

All experiments were performed in a stainless steel, pressure-driven, single-diaphragm shock tube. The driver side had length and diameter of 2.46 m and 7.62 cm, respectively, while the driven side had length and diameter of 4.72 m and 15.24 cm, respectively, where 15.24 cm is the absorption path length. Sidewall pressure traces were recorded 1.6 cm from the endwall using a Kistler 603B1 pressure transducer. The incident-shock velocity was measured via five piezoelectric pressure transducers and extrapolated to the endwall to calculate the temperature and pressure behind the reflected shock wave (T_5 and P_5) using the normal-shock

relations. Using this method, conservative estimates for uncertainties in T_5 and P_5 are 1.0 and 1.8% due to uncertainty in the determination of the shock velocity [24].

Prior to each experiment, the driven side was vacuumed down to $\sim 1 \times 10^{-6}$ kPa via a turbomolecular pump. The fill pressures for experiments below 50 kPa were monitored with a 0–1.3 kPa gauge, while others were monitored with a 0–130 kPa gauge (MKS Baratron). The leak rate was measured to be $\sim 1.3 \times 10^{-4}$ kPa min⁻¹, and diaphragms were typically burst less than 1 min after filling. The 7.509% CO₂/Ar mixture used for all experiments was manometrically prepared in a separate, 40-L mixing tank using the 0–130 kPa gauge. CO₂ and Ar were supplied by Praxair and Airgas with purity levels of 99.999%. The 7.509% CO₂/Ar mixture was chosen to provide adequate absorption levels while keeping Ar as the dominant perturber. Calculations with the Aramco 1.3 chemical kinetics mechanism [25] confirmed that no thermal decomposition of this mixture occurred even at the highest temperatures studied. In addition, despite the higher concentration of CO₂, no signs of reflected-shock bifurcation were noted in the sidewall pressure traces.

The CO₂ behind the reflected shock wave was subject to vibrational relaxation effects. Estimations of the vibrational relaxation time τ_{vib} were made at the lower-temperature, lower-pressure conditions (1158 K, 5.1 kPa) of this study, where τ_{vib} will be at a maximum. At these conditions, calculations according to Nevdakh et al. [26] suggested $\tau_{\text{vib}} \approx 12$ μs , while interpolation of experimental data from Simpson et al. [27] suggested $\tau_{\text{vib}} \approx 40$ μs . To completely avoid τ_{vib} effects, laser data were recorded starting at least 100 μs after the arrival of the reflected shock wave. The effects of τ_{vib} become increasingly negligible at higher pressures, as shown in Fig. 1.

The pressure rise behind the reflected shock wave (dP/dt) is caused by nonideal effects such as shock attenuation and boundary-layer growth and is exacerbated by the presence of CO₂ [28]. For the lower pressure, higher temperature experiments (~ 5 kPa, ~ 1900 K), dP/dt values were as high as 18% ms⁻¹. This value decreased dramatically with

Table 1 Literature values of the temperature exponent n for the CO₂–Ar system

Rotational quanta	n	Temperature range (K)	References
P(20)	0.66 ^a	300–400	Pack [20]
P(6)–P(60)	0.88 ± 0.18	160–300	Brownsword et al. [13]
R(0)–R(80)	0.70	77–296	Thibault et al. [18]
R(0)–R(80)	0.64	296–765	Thibault et al. [18]
R(48), R(50), R(52)	0.61 ± 0.01	296–2290	Wooldridge et al. [21]
R(28), R(76), R(96)	0.51, 0.60, 0.48, ± 0.02	~ 1000 –2000	Spearrin et al. [22]
R(28), P(70)	0.658, 0.694	~ 300 –1200	Farooq et al. [23]
P(77) ^b	0.61 ± 0.04	1158–2017	This work

^a For potential energy surface 2

^b This range is approximate due to complications discussed herein

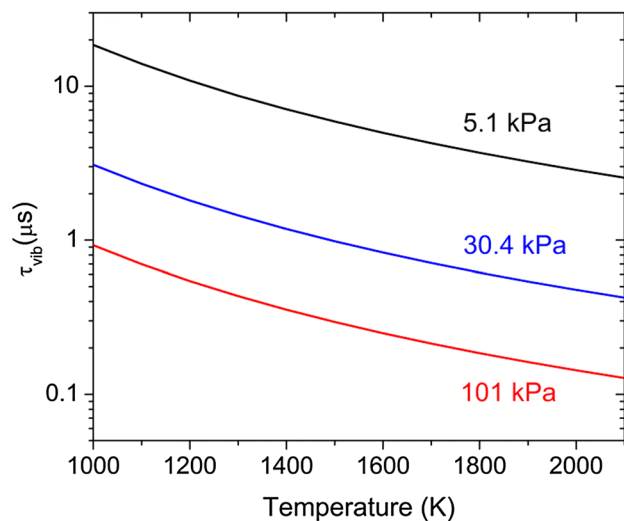


Fig. 1 Estimations of τ_{vib} over a range of temperature at various pressures for a mixture of 7.509% CO_2/Ar . Calculations according to Nevdakh et al. [26]

increasing pressure, however, and for experiments at or above 20 kPa was $\leq 2\% \text{ ms}^{-1}$. To reduce the impact of this nonideality, laser data were taken no later than 800 μs after the reflected shock wave, constraining the measured uncertainty in P_5 due to dP/dt to 14.4% at the lower pressure, higher temperature case. This uncertainty had negligible effect on the determination of $\gamma_{\text{CO}_2-\text{Ar}}(T_0)$, as demonstrated by the error bars shown later in Sect. 5.

3.2 Laser diagnostic

Figure 2 shows a schematic of the laser setup. A quantum cascade laser (QCL) from Alpes Lasers (HHL-L

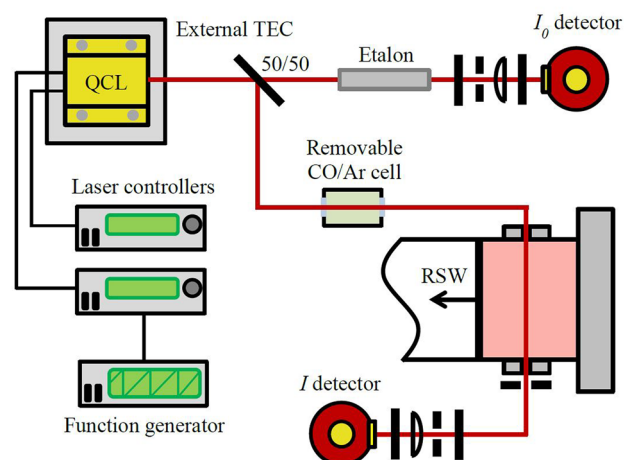


Fig. 2 Schematic of the laser absorption setup used in the scanning experiments

module) was used to generate laser light with a linewidth of $\sim 1.5 \text{ MHz}$, which is ~ 400 times less than the narrowest measured linewidth. The laser was passed through the shock tube via sapphire windows in the same plane as the sidewall pressure transducer. The laser was scanned across a $\sim 0.4 \text{ cm}^{-1}$ range at 2 kHz by modulating the injection current with a sawtooth wave. The center frequency of the laser was controlled by varying the laser temperature between -6 and $-18 \text{ }^\circ\text{C}$. An external cooling plate provided additional laser stability. Two cryogenically cooled InSb detectors (Judson J10D) with bandwidths of 200 kHz monitored I_t and I_{etalon} and were sampled at 1 MHz using a digital oscilloscope. To monitor relative changes in laser frequency, a solid germanium etalon of length 50.8 cm with a free spectral range (FSR) of 0.024 cm^{-1} was placed in front of the I_{etalon} detector. Scan time was converted to relative frequency by fitting a third-order polynomial to the location of the peaks in the I_{etalon} signal. Even at the lowest pressures, where the lines are most narrow, the detector bandwidth and sampling rate were able to adequately capture the shape of the spectra with a spectral resolution of 0.001 cm^{-1} .

The use of Eq. (1) necessitates measurement of both I_t and I_0 , which was accomplished by taking the data from the scan prior to the arrival of the reflected shock wave as I_0 . This baseline intensity was highly repeatable and typically varied by $< 0.4\%$ from scan to scan. Figure 3 shows typical data traces from a scanning experiment. The portions of

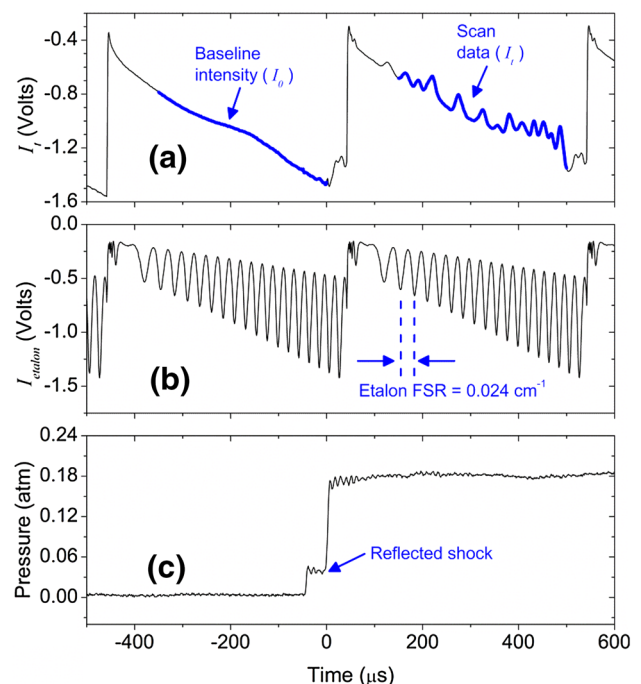


Fig. 3 Sample data traces of the transmitted intensity I_t (a), the etalon intensity I_{etalon} (b), and the sidewall pressure (c) from a scanning experiment at 2017 K and 18.4 kPa in 7.509% CO_2/Ar

the I_t detector trace taken as the baseline intensity (I_0) and scan data (I_t) have been thickened. In accordance with the dP/dt concerns mentioned earlier, the first full scan after the reflected shock was recorded for all experiments.

To convert the relative frequency of the scans to absolute frequency, separate tests were undertaken using a reference line. The location of the strong R(12), $v'' = 0$ line in the fundamental band of CO is given in HITEMP [6] as 2190.0175 cm⁻¹, with an uncertainty between 0.0001 and 0.001 cm⁻¹. An absorption cell was filled with a mixture of ~ 10% CO/Ar, and experiments were carried out with this cell placed in the path of the I_t beam. The sharp CO absorption spike in the resulting measurements was fixed at 2190.0175 cm⁻¹, and the absolute frequencies of the surrounding CO₂ peaks were determined using this known frequency in conjunction with the relative frequency obtained from the I_{etalon} trace. This characterization was performed over the range of temperatures and pressures studied herein to characterize the locations of the CO₂ peaks at different conditions. The absorption cell was filled to a pressure of 1.3 kPa to reduce collisional lineshift of the reference CO line.

Broadband emission from shock-heated gases and shock-tube walls is a source of uncertainty in laser measurements. Narrow bandpass filters (center wavelength 4.5 μm , FWHM 0.5 μm) and irises were utilized to reduce this emission. Since the emission could not be completely eliminated, a series of experiments were carried out to characterize the background emission as a function of T_5 and P_5 . Experiments were run with the laser turned off, and the resulting emission level (typically 0.5–10.0 mV) in the I_t detector was recorded. Correlations of the emission versus T_5 and P_5 were obtained and used to correct all CO₂ spectra; corrections slightly increased CO₂ percent absorption levels by a relative change of 1.0–2.2%.

4 Results and analysis

4.1 Experimental profiles

Figure 4 shows typical experimental results. The presence of several distinct CO₂ lines is evident, although, as discussed later, there are many more lines present than is immediately evident. Also depicted in Fig. 4 are the bounds due to uncertainty in background emission and detector offset. A slight detector offset was measured to be -11 mV for the I_t detector and was taken into account in post-processing. Highly conservative estimates of uncertainty in emission ($\pm 20\%$) and detector offset (± 10 mV) were used to calculate the dashed lines in Fig. 4, and yet, the relative difference between experiment and uncertainty calculations is still only $\leq 1.5\%$ at all points.

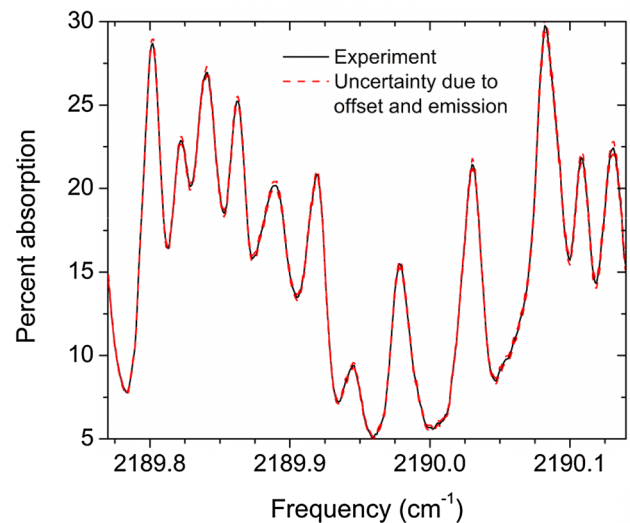


Fig. 4 Percent absorption versus absolute frequency for an experiment at the conditions of Fig. 3. Dashed lines are uncertainty limits due to uncertainty in emission and offset and are nearly indistinguishable from the experiment

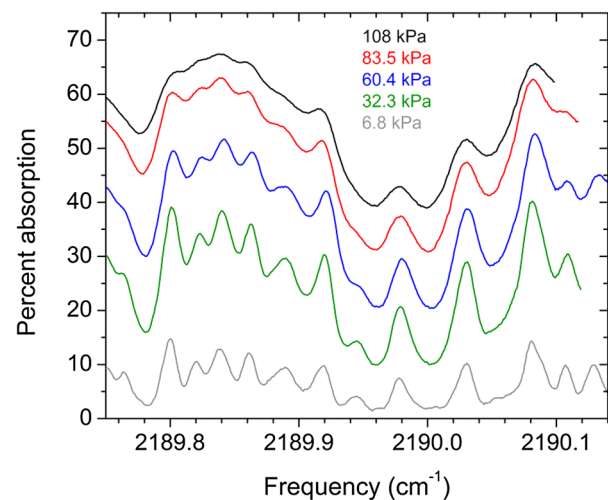


Fig. 5 Measured spectra at varying pressures in a mixture of 7.509% CO₂/Ar. The temperature is 1910 ± 70 K

The effect of pressure on measured spectra is shown in Fig. 5 for several experiments at similar temperatures. As expected, the spectra become more broadened with increasing pressure. Note that the increasing absorption is almost entirely due to growth of the P term in Eq. (1) rather than shock-to-shock variations in temperature. Figure 6 shows the effect of temperature for experiments at similar pressures. The absorption was found to increase with temperature for all frequency regions of this study. Although a discussion of linestrengths is outside of the scope of this study, the increasing absorption is likely due to the presence of many

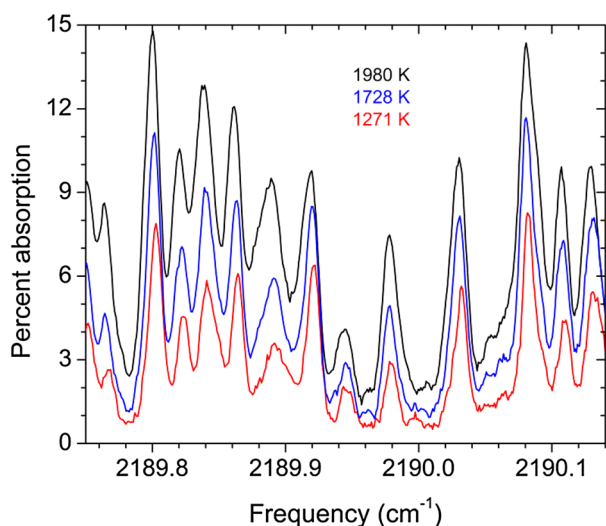


Fig. 6 Measured spectra at varying temperatures in a mixture of 7.509% CO₂/Ar. The pressure is 7.5 ± 1.4 kPa

underlying hot bands that become increasingly populated with increasing temperature.

Experiments performed near 2190.0 cm^{-1} had low uncertainty in absolute frequency ($\pm 0.001 \text{ cm}^{-1}$) due to the proximity of the reference CO line. For experiments farther from this line, similar spectral features at overlapping frequencies were compared (starting from experiments near 2190.0 cm^{-1}) and used to assign absolute frequencies with an estimated uncertainty of $\pm 0.005 \text{ cm}^{-1}$. This uncertainty arises from the uncertainty in aligning similar features as well as the uncertainty in line-shift effects due to temperature and pressure. The full set of measured spectra is provided in the Supplementary Material.

4.2 Optimization routine

4.2.1 General principle

Modeling of measured spectra with HITRAN 2004 [1], HITRAN 2012 [2], and CDSD-296 [3] gave extremely poor results. HITEMP [6], however, showed good agreement with measured spectra, as shown in Fig. 7. The HITEMP database was specifically developed for high-temperature applications through inclusion of many hot bands that are excluded in the other databases. Figure 7 demonstrates the potential pitfalls of using a spectroscopic database far from its intended temperature range, particularly in frequency regions with hot bands.

To extract broadening information from the data, an optimization routine was implemented to minimize differences between measured and modeled spectra, using HITEMP as a starting point. The optimization was performed for each

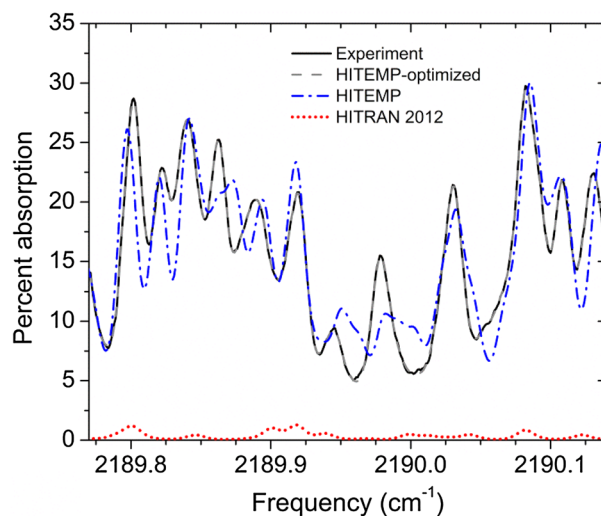


Fig. 7 Experimental results at the conditions in Fig. 3. The optimized HITEMP values are indistinguishable from the experiment. Not shown are HITRAN 2004 and CDSD-296 as they yielded nearly identical results to HITRAN 2012

individual experiment, although only experiments near 2190.0 cm^{-1} were optimized due to lower uncertainty in absolute wavelength. Three types of variables were allowed to vary: the linestrength of each line, the position of each line, and a global value of $\Delta\nu_L$ for all lines within the experiment.

Justification for use of a global $\Delta\nu_L$ across all lines in this region is twofold. First, as previously mentioned (Sect. 2.2), there is general agreement that $\gamma_{\text{CO}_2\text{-Ar}}(T_0)$ is independent of the vibrational band. The contribution of many hot bands should, therefore, still allow for a global $\Delta\nu_L$. Second, at high temperatures and high J'' , broadening coefficients of CO₂ by various molecules (including CO₂ itself) become independent of J'' [29]. Temperatures in this study were all greater than 1150 K. Optimized lines near 2190.0 cm^{-1} had high J'' values, typically from about 50–90, although values as high as 127 were noted.

Sample optimization results are shown in Fig. 7. Through optimization of linestrengths, line positions, and the global value of $\Delta\nu_L$, the optimization achieved excellent agreement with the experiment. For this experiment, an optimized value of 0.0040 cm^{-1} was obtained for $\Delta\nu_L$.

4.2.2 Initial guesses and bounds

The initial guess for the linestrength of each line was the calculated linestrength at the experimental T_5 using $S(296\text{K})$ from HITEMP and the partition function according to [30]. The bounds for the linestrength were based on the uncertainty indices given in HITEMP. For lines with a stated

uncertainty of ≥ 20%, the linestrength was allowed to vary within a factor of 1.4.

The initial guess for the line position of each line was the HITEMP value of the line position. The bounds for the line position were based on the uncertainty indices given in HITEMP, but were conservatively given a maximum value of ± 0.05 cm⁻¹, although most lines in this frequency region have a stated uncertainty of up to ± 0.1 cm⁻¹.

The initial guess for Δν_L was set at the value calculated from Wooldridge et al. [21]. The bounds for Δν_L were arbitrarily set to within a factor of three of the Wooldridge value; all optimized values of Δν_L fell well within these bounds, thereby avoiding constraint effects on the optimization. The value of Δν_D for each line was calculated according to Eq. (2). The lineshape calculation was performed according to the Voigt approximation by Liu et al. [31].

Lines with an initially calculated linestrength below about 0.001 cm⁻² atm.⁻¹ were excluded from the optimization, but were included in the calculation of the final objective function. For these non-optimized lines, the line position was fixed at the HITEMP value and the value of Δν_L was fixed at the value calculated from Wooldridge et al. [21]. This simplification was necessary due to the large number of lines contained within HITEMP. For example, for the frequency range (~ 0.4 cm⁻¹) shown in Fig. 7, HITEMP contains ~ 3700 lines. Most of these lines are negligibly weak at the experimental T₅, and a line-strength cutoff of 0.002 cm⁻² atm.⁻¹ reduces this to 48 optimized lines, making the optimization computationally feasible. It should be stressed once again that the non-optimized lines were still included in calculations of the objective function, and that it is this large number of lines that makes HITEMP more accurate at higher temperatures than certain other databases. Shown in Table 2 is the number of lines and maximum linestrength at 1500 K in a selected frequency region for four databases. It is seen that HITEMP has a much higher number of lines and a higher maximum linestrength due to the inclusion of hot bands. CDSD-1000 [4] and the more modern CDSD-4000 [5] were not considered due to the recommendation by the authors of [5] that HITEMP be used for temperatures below 2000 K.

Table 2 Spectroscopic database parameters in the frequency range 2188.5–2193.0 cm⁻¹

Database name	Number of lines	S _{max} at 1500 K (cm ⁻² atm. ⁻¹)
HITRAN 2004	75	2.08 × 10 ⁻³
HITRAN 2012	701	2.17 × 10 ⁻³
CDSD-296	928	2.17 × 10 ⁻³
HITEMP	43,440	8.42 × 10 ⁻³

5 Broadening coefficient results and discussion

5.1 Extraction of γ_{CO₂-Ar}(T₀) and n

The optimized values of Δν_L still contain self-broadening from CO₂ due to the non-negligible concentration (7.509%) of CO₂ in the mixture. To remove the self-broadening portion of Δν_L, relations for CO₂ self-broadening based on Eq. (3) and Rosenmann et al. [29] were used:

$$\Delta\nu_{L,CO_2-CO_2} = 2\gamma_{300} \left(\frac{300}{T}\right)^N P X_{CO_2} \tag{5}$$

and

$$N = N_{300} \left(\frac{300}{T}\right)^\alpha \tag{6}$$

Here, Δν_{L,CO₂-CO₂} is the self-broadened Lorentzian FWHM; X_{CO₂} is the mole fraction of CO₂; and γ₃₀₀, N₃₀₀, and α are constants given by [29]. These constants assume a value of CO₂ self-broadening that is independent of J'', as was assumed in the optimization. The Ar-broadened FWHM, Δν_{L,CO₂-Ar}, can then be calculated via

$$\Delta\nu_{L,CO_2-Ar} = \Delta\nu_L - \Delta\nu_{L,CO_2-CO_2} \tag{7}$$

The values of Δν_{L,CO₂-Ar} obtained from the optimized values of Δν_L and Eq. (7) are shown in Fig. 8 as a function of pressure. As expected based on Eq. (3), a linear relationship with pressure is evident in the data. Similarly, Fig. 9 shows the behavior of Δν_{L,CO₂-Ar} versus temperature. The data appear linear on a log scale, confirming the power law behavior described in Eq. (4). Error bars on the y-axis in Figs. 8 and 9 were estimated at ± 12 and ± 10%, respectively, based

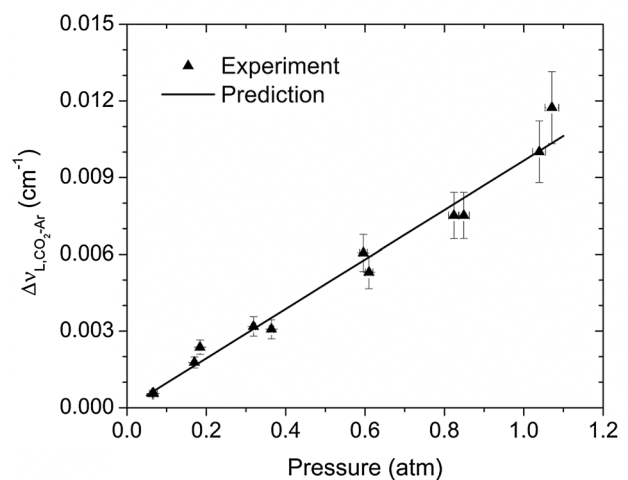


Fig. 8 Effect of pressure on the Lorentzian linewidth due to CO₂-Ar broadening in 7.509% CO₂/Ar. All data points were adjusted to the average temperature of 1908 K for this plot. Solid line is the prediction according to the proposed broadening parameters

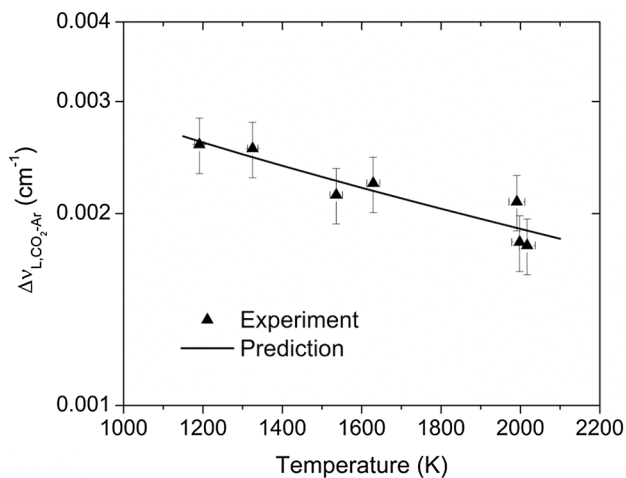


Fig. 9 Effect of temperature on the Lorentzian linewidth due to $\text{CO}_2\text{-Ar}$ broadening in 7.509% CO_2/Ar . All data points were adjusted to the average pressure of 20.3 kPa for this plot. Solid line is the prediction according to the proposed broadening parameters

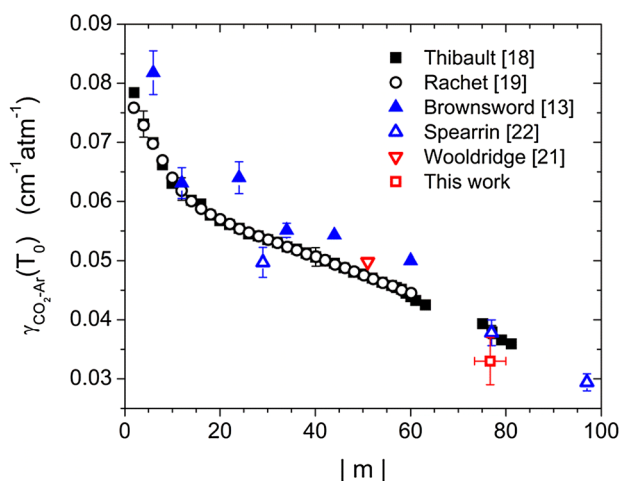


Fig. 10 Historical and present values of $\gamma_{\text{CO}_2\text{-Ar}}(T_0)$. The x -axis is the absolute value of the spectroscopic parameter m , where $m = J'' + 1$ for R-branch lines and $m = -J''$ for P-branch lines

on the scatter in the data and the uncertainty introduced by the subtraction of the CO_2 self-broadening. Uncertainties in pressure in Fig. 8 are due to measured dP/dt values (Sect. 3.1). From the data plotted in Figs. 8 and 9, best-fit values of $\gamma_{\text{CO}_2\text{-Ar}}(T_0) = 0.033 \pm 0.004$ and $n = 0.61 \pm 0.04$ were obtained.

5.2 Comparison to historical data

Values of $\gamma_{\text{CO}_2\text{-Ar}}(T_0)$ from the literature are compared to the present work, as shown in Fig. 10. The consensus on the J'' dependence of $\gamma_{\text{CO}_2\text{-Ar}}(T_0)$ can be seen in

the excellent agreement between Thibault et al. [18] and Rachet et al. [19]. Note also that the Thibault et al. and Rachet et al. measurements were made in different vibrational bands, confirming the lack of vibrational dependence mentioned earlier. The Brownsword et al. [13] measurements show less agreement with this consensus value and also have a value of n that is noticeably different from other workers (Table 1).

The single value provided by Wooldridge et al. [21] was made directly at 296 K in addition to measurements up to 2290 K. On the other hand, the value provided by this work and the three values provided by Spearrin et al. [22] were made at high temperatures and extrapolated to 296 K via the exponent n . Nonetheless, both the present work and Spearrin et al. are within 12% of historical measurements of $\gamma_{\text{CO}_2\text{-Ar}}(T_0)$ at 296 K.

Previous evaluations of the temperature exponent n are shown in Table 1. The value from the present work is in excellent agreement with Wooldridge et al. [21] and the R(76) results from Spearrin et al. [22]. Good agreement is also seen with the theoretical predictions from Pack [20] and the high-temperature measurements/predictions from Thibault et al. [18]. As previously mentioned, the discrepancy between Brownsword et al. [13] and the remaining literature values is likely due to the lower temperature range studied by Brownsword et al.

As mentioned in Sect. 4.2.1, values obtained in the present work were averaged over many different rotational lines. To determine the average J'' , a linestrength-weighted average of the J'' values for each optimized line was performed for each experiment, yielding a value of $J'' = 76.7 \pm 3.3$; this explains the x -axis error bars on the present work, as shown in Fig. 10. Consequently, it should be stressed that the current results only represent an averaged $\text{CO}_2\text{-Ar}$ broadening coefficient in the region near 2190.0 cm^{-1} .

5.3 Line-mixing effects

Collisional line mixing is a phenomenon that can significantly alter spectra and has been previously studied for CO_2 (see [32] and references therein). Line mixing occurs when “collisions transfer absorbers from weakly absorbing regions to strongly absorbing regions leading to a narrowing of spectral structure” [7] and becomes significant at higher number densities and with tighter spacing between lines of the same band [33]. Previous work has shown that CO_2 line mixing is of no consequence at ~ 0.92 amagat near 3600 cm^{-1} [32]. Since the number densities for the experiments herein ranged from 0.01 to 0.16 amagat, line-mixing effects can be neglected, and the use of the Voigt profile is justified.

6 Fixed-wavelength experiments

6.1 CO₂/Ar experiments

To test the ability of the current results to predict CO₂ absorption levels at the R(12), $v'' = 0$ line of CO, a series of fixed-wavelength experiments were carried out over a range of temperatures (1150–2050 K) and pressures (122, 446, and 1115 kPa). The experimental setup was identical to that described above (Fig. 2) save for two differences: the frequency of the laser was fixed and the etalon was removed from the setup. The laser was scanned over the R(12) CO transition and fixed at the peak of 2190.0175 cm⁻¹ prior to each experiment through use of the removable absorption cell. Post-shock checks revealed no signs of laser drift during the course of an experiment.

In a similar manner as the scanning tests, broadband emission entering the I_t detector was characterized as a function of temperature for each pressure range. Emission measurements for 122 and 446 kPa are shown in Fig. 11. Using linear fits to the emission measurements, predicted emission for each absorption experiment was subtracted from I_t in post-processing. Slight detector offsets were also accounted for.

Experiments at 122 and 446 kPa were performed with a mixture of 1.748% CO₂/Ar. For the 1115-kPa experiments, a mixture of 1.165% CO₂/Ar was used to avoid optical thickness complications. For both mixtures, calculations of τ_{vib} according to [26] yielded $\tau_{vib} \leq 1 \mu s$ for all conditions and thus vibrational relaxation effects were not considered.

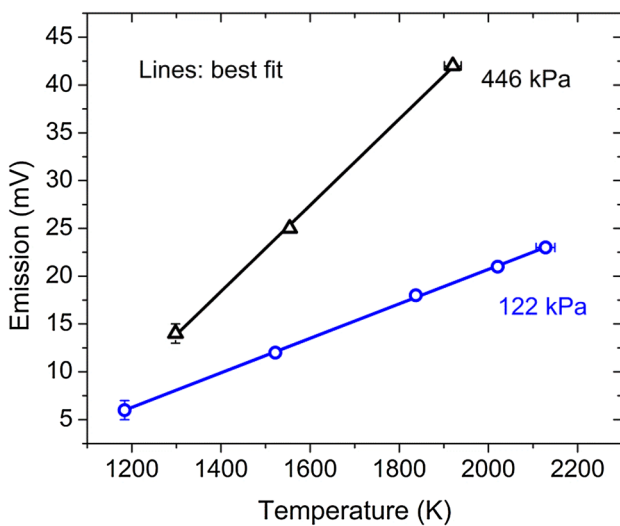


Fig. 11 Broadband emission entering the I_t detector as a function of temperature for two different average pressures in a mixture of 1.748% CO₂/Ar

A sample experiment is shown in Fig. 12. In agreement with predictions from HITEMP, no absorption was observed prior to the incident shock. A slight rise in absorption can be seen behind the reflected shock due to nonideal dP/dt . The effect of this nonideality was eliminated by taking the absorption level immediately after the reflected shock.

The fixed-wavelength results are shown in Fig. 13 along with predictions from HITEMP. These predictions utilized

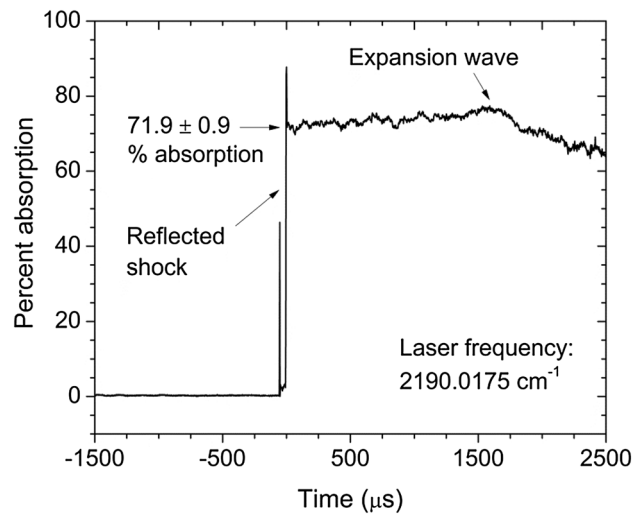


Fig. 12 Absorption time history for an experiment at 1854 K and 1079 kPa in a mixture of 1.165% CO₂/Ar. The path length is 15.24 cm, yielding an absorption coefficient of $0.672 \pm 0.016 \text{ cm}^{-1} \text{ atm}^{-1}$.

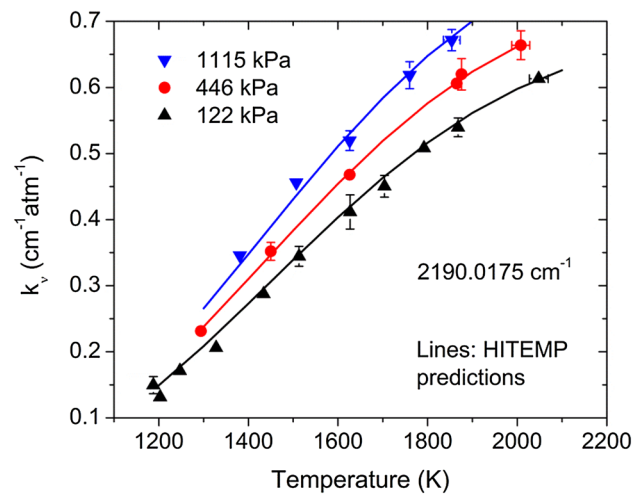


Fig. 13 Experimental and modeled absorption coefficients at 2190.0175 cm⁻¹ versus temperature at various pressures. Solid lines are HITEMP predictions incorporating the broadening from the present work and the measured lineshift for the nearest CO₂ line. Uncertainty in the y-axis is due to noise in the signal and is smaller than the size of the symbol if not visible

the CO₂–Ar broadening parameters proposed herein along with the J'' -independent self-broadening parameters from [29]. In addition, the lineshift of the CO₂ peak nearest to 2190.0175 cm⁻¹ (the peak at 2190.22 cm⁻¹ in Fig. 7) was measured during the tests mentioned in Sect. 3.2 and was determined to be $\Delta\nu_s = 0.00424X_{\text{Ar}}P(T_0/T)^{0.40}$, where $\Delta\nu_s$ is the lineshift [cm⁻¹]. This lineshift was incorporated into the calculations, as displayed in Fig. 13.

Neglecting the lineshift and using the broadening parameters from Wooldridge et al. [21] yield predictions at 122 kPa that are consistently ~ 6.3% higher than those shown in Fig. 13. This difference is well outside of the measurement uncertainty of the data and falls closer to the 446-kPa data than the 122-kPa data, demonstrating the importance of accurate lineshape modeling.

The experiments at 1115 kPa have number densities between 1.57 and 2.21 amagat. At these number densities, line-mixing effects may no longer be insignificant as in the 122-kPa tests or in the scanning tests. Nonetheless, Fig. 13 still demonstrates excellent agreement between data and predictions. Thus, for the purposes of modeling k_v of CO₂ at 2190.0175 cm⁻¹, using HITEMP with the broadening and lineshift parameters or interpolating between the experimental data of Fig. 13 will both yield accurate results.

6.2 CH₄/C₂H₆ experiments

The k_v data at 2190.0175 cm⁻¹ (Fig. 13) were recently implemented in a study from the authors' laboratory [9]. This study measured CO time histories during the oxidation of a fuel-lean ($\phi = 0.5$) CH₄/C₂H₆ blend diluted in 99% Ar. The experimental setup was identical to that described in Sect. 6.1. A sample experiment is shown in Fig. 14, during which the mixture was shock heated and, after a very short induction period, began to form and then consume CO as combustion progressed.

Initial CO measurements that did not account for interfering CO₂ absorption showed significantly higher levels of CO in the tail of the time history than was predicted by a modern chemical kinetics mechanism. However, correcting for CO₂ absorption using the k_v data from Fig. 13 and the predicted CO₂ profiles from the chemical kinetics mechanism yielded much better agreement with the mechanism, as shown in Fig. 14. The significant correction to the CO profile results from the fact that k_v for CO decreases with increasing T_5 and P_5 , while k_v for CO₂ shows the opposite trend, making the two k_v values comparable at the conditions of Fig. 14. Corrections at lower T_5 , P_5 are much less significant. Note that the shape of the predicted CO₂ profile (the dotted line in Fig. 14) for similar mixtures has also been confirmed experimentally using a CO₂ emission diagnostic. Thus, the present results should be useful in correcting for interfering absorption from CO₂ during chemical kinetics experiments.

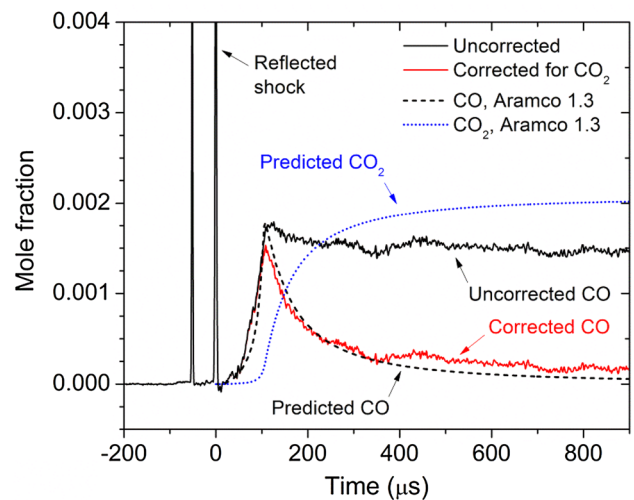


Fig. 14 Measured and predicted CO time-histories during oxidation of a fuel-lean ($\phi = 0.5$) mixture of CH₄/C₂H₆ in 99% Ar at 1737 K and 1099 kPa. The predicted k_v for CO₂ at these conditions is 0.592 cm⁻¹ atm⁻¹. Data are from [9], while the model predictions (dashed line and dotted line) are from [25]

7 Conclusions

Ar-diluted CO₂ spectra were recorded between 1158 and 2017 K at pressures between 5.1 and 108 kPa using a scanned-wavelength laser diagnostic between 2188.8 and 2191.8 cm⁻¹. HITRAN 2004, HITRAN 2012, and CDSD-296 were all found to severely underpredict the data. HITEMP, however, provided much better predictions, highlighting the need for caution in selecting a spectral database for simulating high-temperature spectra. Spectra near 2190.0 cm⁻¹ were analyzed using an optimization routine to extract Ar-broadening information from the data. The spectra were simulated with the Voigt profile due to low number densities in these experiments that should eliminate line-mixing effects.

The optimized broadening parameters of 0.033 cm⁻¹ atm⁻¹ and 0.61 for $\gamma_{\text{CO}_2\text{-Ar}}(T_0)$ and n agree well with historical data assuming an effective J'' value of 76.7 for the experiments near 2190.0 cm⁻¹. These values should be accurate at 2190.0 ± 0.2 cm⁻¹ and within the temperature range of 1150–2050 K and may be useful beyond these ranges. Fixed-wavelength experiments were also conducted at 2190.0175 cm⁻¹ in CO₂/Ar mixtures at 122, 446, and 1115 kPa and between 1100 and 2100 K. The measured k_v data show excellent agreement with predictions from HITEMP using the proposed broadening data along with a slight lineshift. These k_v data for CO₂ were shown to be successful in correcting CO time histories measured in chemical kinetics experiments.

Acknowledgements The authors would like to thank the NSF for funding this work (Grant DGE-1252521) and also Sulaiman Al Turaifi for his help in performing some of the experiments.

References

1. L.S. Rothman, D. Jacquemart, A. Barbe, D. Chris Benner, M. Birk, L.R. Brown et al., *JQSRT* **96**, 139 (2005)
2. L.S. Rothman, I.E. Gordon, Y. Babikov, A. Barbe, D. Chris Benner, P.F. Bernath et al., *JQSRT* **130**, 4 (2013)
3. S.A. Tashkun, V.I. Perevalov, R.R. Gamache, J. Lamouroux, *JQSRT* **152**, 45 (2015)
4. S.A. Tashkun, V.I. Perevalov, J.-L. Teffo, A.D. Bykov, N.N. Lavrentieva, *JQSRT* **82**, 165 (2003)
5. S.A. Tashkun, V.I. Perevalov, *JQSRT* **112**, 1403 (2011)
6. L.S. Rothman, I.E. Gordon, R.J. Barber, H. Dothe, R.R. Gamache, A. Goldman et al., *JQSRT* **111**, 2139 (2010)
7. C.S. Goldenstein, R.M. Spearrin, J.B. Jeffries, R.K. Hanson, *Prog. Energy Combust. Sci.* **60**, 132 (2017)
8. E.L. Petersen, R.K. Hanson, *Shock Waves* **15**, 333 (2006)
9. O. Mathieu, C.R. Mulvihill, E.L. Petersen, Y. Zhang, H.J. Curran, *J. Eng. Gas Turbines Power* **139**(12), 121507-1–121507-8 (2017)
10. W. Ren, A. Farooq, D.F. Davidson, R.K. Hanson, *Appl. Phys. B* **107**, 849 (2012)
11. C. Boulet, P. Isnard, E. Arié, *JQSRT* **14**, 637 (1974)
12. F. Thibault, J. Boissoles, R. Le Doucen, J.P. Bouanich, P. Arcas, C. Boulet, *J. Chem. Phys.* **96**, 4945 (1992)
13. R.A. Brownsword, J.S. Salh, I.W.M. Smith, *J. Chem. Soc. Faraday Trans.* **91**, 191 (1995)
14. B. Khalil, F. Thibault, J. Boissoles, *Chem. Phys. Lett.* **284**, 230 (1998)
15. D.C. Benner, C.E. Miller, V.M. Devi, *Can. J. Phys.* **87**, 499 (2009)
16. J. Buldyreva, M. Chrysos, *J. Chem. Phys.* **115**, 7436 (2001)
17. E. Arié, N. Lacombe, P. Arcas, A. Levy, *Appl. Opt.* **25**, 2584 (1986)
18. F. Thibault, B. Calil, J. Buldyreva, M. Chrysos, J.M. Hartmann, J.P. Bouanich, *Phys. Chem. Chem. Phys.* **3**, 3924 (2001)
19. F. Rachet, M. Margottin-Maclou, A. Henry, A. Valentin, *J. Mol. Spectrosc.* **175**, 315 (1996)
20. R.T. Pack, *J. Chem. Phys.* **70**, 3424 (1979)
21. M.S. Wooldridge, R.K. Hanson, C.T. Bowman, *JQSRT* **57**, 425 (1997)
22. R.M. Spearrin, W. Ren, J.B. Jeffries, R.K. Hanson, *Appl. Phys. B* **116**, 855 (2014)
23. A. Farooq, J.B. Jeffries, R.K. Hanson, *Appl. Phys. B* **90**, 619 (2008)
24. E.L. Petersen, M.J. Rickard, M.W. Crofton, E.D. Abbey, M.J. Traum, D.M. Kalitan, *Meas. Sci. Technol.* **16**, 1716 (2005)
25. W.K. Metcalfe, S.M. Burke, S.S. Ahmed, H.J. Curran, *Int. J. Chem. Kinet.* **45**, 638 (2013)
26. V.V. Nevdakh, L.N. Orlov, N.S. Leshenyuk, *J. Appl. Spectrosc.* **70**, 276 (2003)
27. C.J.S.M. Simpson, T.R.D. Chandler, A.C. Strawson, *J. Chem. Phys.* **51**, 2214 (1969)
28. J.W. Hargis, E.L. Petersen, *AIAA J.* **55**, 902 (2017)
29. L. Rosenmann, J.M. Hartmann, M.Y. Perrin, J. Taine, *Appl. Opt.* **27**, 3902 (1988)
30. A.L. Laraia, R.R. Gamache, J. Lamouroux, I.E. Gordon, L.S. Rothman, *Icarus* **215**, 391 (2011)
31. Y.Y. Liu, J.L. Lin, G.M. Huang, Y.Q. Guo, C.X. Duan, *J. Opt. Soc. Am. B* **18**, 666 (2001)
32. A. Farooq, J.B. Jeffries, R.K. Hanson, *JQSRT* **111**, 949 (2010)
33. J.-M. Hartmann, C. Boulet, D. Robert, *Collisional Effects on Molecular Spectra* (Elsevier, Amsterdam, 2008)